IOP Publishing New J. Phys. 28 (2026) 064302 https://doi.org/10.1088/1367-2630/ae7c29

New Journal of Physics
The open access journal at the forefront of physics

Published in partnership with: Deutsche Physikalische Gesellschaft and the Institute of Physics

OPEN ACCESS

RECEIVED
29 January 2026

REVISED
4 June 2026

ACCEPTED FOR PUBLICATION
11 June 2026

PUBLISHED
23 June 2026

PAPER

Photon accelerator in magnetized electron–ion plasma

S V Bulanov[1], S S Bulanov[2], T Z Esirkepov[3], G Gregori[4], G M Grittani[1], M Lamač[1], B K Russell[5], A G R Thomas[6] and P Valenta[1,*]

[1] ELI Beamlines Facility, Extreme Light Infrastructure ERIC, Dolní Břežany, Czech Republic
[2] Lawrence Berkeley National Laboratory, Berkeley, CA, United States of America
[3] Kansai Institute for Photon Science, National Institutes for Quantum Science and Technology, Kyoto, Japan
[4] Department of Physics, University of Oxford, Oxford, United Kingdom
[5] Department of Astrophysical Sciences, Princeton University, Princeton, NJ, United States of America
[6] Gerard Mourou Center for Ultrafast Optical Science, University of Michigan, Ann Arbor, MI, United States of America
[*] Author to whom any correspondence should be addressed.

E-mail: petr.valenta@eli-beams.eu

Keywords: photon accelerator, magnetized plasma, frequency upshifting

Abstract

Strong magnetic fields and plasmas are intrinsically linked in both terrestrial laboratory experiments and in space phenomena. One of the most profound consequences of that is the change in relationship between the frequency and the wave number of electromagnetic waves propagating in plasma in the presence of such magnetic fields when compared to the case without these fields. Furthermore, magnetic fields alter electromagnetic wave interaction with relativistic plasma waves, resulting in different outcomes for particle and radiation generation. For a relativistic plasma wave-based photon acceleration this leads to an increased frequency gain and, thus, potentially to higher efficiency. The influence of a magnetic field leads to quantitative and qualitative change in the properties of photon acceleration, amplifying the increase in the electromagnetic wave frequency.

1. Introduction

The interaction of intense electromagnetic waves with plasmas of different density and composition almost necessarily leads to the generation of electron density modulations, which can have different properties, including velocities ranging from non-relativistic to relativistic ones. In a rarefied plasma, the relativistic speed of these density modulations is approximately equal to the group velocity of the electromagnetic wave. The interaction of these density modulations with electromagnetic waves, whether with the waves that generated these modulations or with other waves, results in a change in the amplitude and frequency of the waves. In the case of increasing frequency and amplitude of the wave, this process has been called 'photon acceleration', a term introduced by Wilks *et al* in 1989 [1] (see also [2] as well as [3–9]). A frequency-upshifted and highly intense electromagnetic pulse from a 'photon accelerator' and/or an x-ray free-electron laser can, in principle, be used to study otherwise inaccessible regimes of strong-field quantum electrodynamics [10] in collisions with high-energy electron beams [11].

Typically, when an electromagnetic wave transfers energy into plasma, a process known as wake wave generation occurs. This process belongs to the range of problems associated with the interaction of electromagnetic waves with plasma waves, which, from a more general point of view, includes the study of the transformation of waves of different types and parametric instabilities, as well as stimulated Raman scattering of light. Below, we consider only those aspects of photon interactions with wake waves that are directly related to 'photon acceleration'.

Wake waves are actively studied in connection with laser acceleration of electrons within the framework of the laser wakefield acceleration paradigm [12–17]. The universal nature of wake acceleration has made it attractive for applications in accelerating high-energy charged particles in space (see [18–20] where this mechanism is considered in relation to cosmic ray acceleration). In fact, the idea of using a wake plasma wave to increase the frequency of electromagnetic waves and amplify them originated in laboratory laser plasmas and was first considered for 'photon acceleration' [1] and 'relativistic flying mirrors' [21] assuming that electron density modulations in the plasma are driven by a short laser pulse. In what we will consider below, this is a necessary condition, but not a sufficient one, since what is most important is to have a configuration in which the electromagnetic wave interacts with refractive index modulations moving at relativistic speed, which can be in the form of relativistic electron layers, relativistic shock waves, etc (see [22, 23]). For simplicity, we will use the term 'wake wave' in all these cases from now on.

Since the amplification of electromagnetic waves with increasing frequency is studied as one of the main mechanisms of high-energy electromagnetic bursts (e.g. in particular, Lorimer radio bursts: [24–26]) generated during supernova explosions and in the magnetospheres of pulsars and magnetars (see [22, 23, 27–30]), it is advisable to expand the photon acceleration paradigm to construct a theory of the emission of intense coherent radiation during cosmic active processes.

In space environment, plasma is almost always embedded in a strong magnetic field that alters the dispersion equation, which determines the relationship between the electromagnetic wave frequency and wave number, compared to the typical case of a relativistic laser plasma [31]. The magnetic field playing important role in relativistic laser plasma [32, 33] is known to change wakefield acceleration of charged particles [4, 33]. Although the effects of magnetic fields on photon accelerators has been considered previously (see, e.g. [2, 34]), here we present a systematic consideration based on an analysis of the structure of the phase space of dynamical systems possessing conserved integrals. It is shown that magnetic field effects lead to both qualitative and quantitative changes in the process of photon acceleration compared to the case of non-magnetized plasma.

2. Photon acceleration for linearly polarized electromagnetic waves propagating across a magnetic field

To describe the propagation of a short-wavelength packet of electromagnetic radiation through a plasma, one can use the geometric optics approximation, which is the subject of many works (see, e.g. [35–38] and references therein). As is well known, geometric optics approximation is closely related to the Wentzel–Kramers–Brillouin approximation [39, 40]. The equations of the wave-packet motion described by the coordinate x (the center of the wave packet) and momentum k (carrier wave vector) read as follows

$$\dot{k} = -\partial_x \omega \quad \text{and} \quad \dot{x} = \partial_k \omega, \tag{1}$$

where ∂_x and ∂_k are the partial derivatives with respect to the coordinate and wave number, respectively, and ω is the wave frequency. In this expression $\partial_k \omega$ is the group velocity v_g of the electromagnetic wave. The wave phase velocity is $v_{ph} = \omega/k$. Here and below the dot stands for the derivative with respect to time, t. The wave packet frequency dependence on the wave number and plasma parameters depends on whether or not the plasma is magnetized.

Below we consider the case when the linearly polarized electromagnetic pulse interacts with collisionless plasma embedded to the homogeneous magnetic field assuming that the wave vector of the wave and magnetic field are perpendicular to each other. The dispersion equations, which determine the relationship between wave number and frequency for linearly polarized electromagnetic waves, depend on whether the electric field vector is directed along or perpendicular to the magnetic field.

2.1. Ordinary electromagnetic wave

In the first case of so-called ordinary wave (O-wave), when the electric field vector is directed perpendicular to the magnetic field, the dispersion equation is given by

$$\omega(x,k,t) = \sqrt{k^2c^2 + \omega_{pe}^2(k_w(x - v_w t))}. \tag{2}$$

Here $\omega_{pe}(k_w(x - v_w t)) = \sqrt{4\pi e^2 n(k_w(x - v_w t))/m_e}$ is the plasma frequency of the wake wave propagating along the x-direction with the phase velocity v_w, e and m_e are the electron charge and mass, respectively, c is the speed of light in vacuum, $n(k_w(x - v_w t))$ is the electron density, and k_w is the inverse scale length of the configuration inhomogeneity. Dispersion equation (2) is the same as in the case of the interaction of an electromagnetic wave with a collisionless non-magnetized plasma [39], so the results presented in the next section are also applicable to this case.

2.1.1. Lagrangian of 'massive photon' and Jacobi integral

Using expression (2) we can write equations (1) in the form

$$\dot{k} = -\frac{\omega_{\rm pe}\partial_x\omega_{\rm pe}}{\sqrt{k^2c^2 + \omega_{\rm pe}\left(k_{\rm w}\left(x - v_{\rm w}t\right)\right)}} \quad \text{and} \quad \dot{x} = \frac{kc^2}{\sqrt{k^2c^2 + \omega_{\rm pe}^2\left(k_{\rm w}\left(x - v_{\rm w}t\right)\right)}}. \tag{3}$$

We can find the wave number and wave frequency as functions of the wave packet velocity $\dot{x}$:

$$k = \frac{\left(\omega_{\rm pe}/c^2\right)\dot{x}}{\sqrt{1 - \dot{x}^2/c^2}} \quad \text{and} \quad \omega = \frac{\omega_{\rm pe}}{\sqrt{1 - \dot{x}^2/c^2}}. \tag{4}$$

The equation of the wave-packet motion takes the form

$$\frac{\mathrm{d}}{\mathrm{d}t}\left[\frac{\left(\omega_{\rm pe}/c^2\right)\dot{x}}{\sqrt{1 - \dot{x}^2/c^2}}\right] = -\sqrt{1 - \dot{x}^2/c^2}\,\partial_x\omega, \tag{5}$$

which is the Euler–Lagrange equation

$$\frac{\mathrm{d}}{\mathrm{d}t}\left(\frac{\partial\mathcal{L}}{\partial\dot{x}}\right) - \frac{\partial\mathcal{L}}{\partial x} = 0 \tag{6}$$

for the Lagrangian

$$\mathcal{L} = -\omega_{\rm pe}\sqrt{1 - \dot{x}^2/c^2}. \tag{7}$$

It has a form of the Lagrangian of relativistic particle (see, e.g. [41]) having a 'mas' equal to the Langmuir frequency [42], which depends on the coordinate and time as $\omega_{\rm pe}\left(k_{\rm w}\left(x - v_{\rm w}t\right)\right)$.

Below we use dimensionless variables normalized on

$$k_{\rm w}^{-1},\ \left(k_{\rm w}c\right)^{-1},\ k_{\rm w}c,\ k_{\rm w} \tag{8}$$

for coordinate x, time t, frequency ω, and wave number k, respectively. Introducing a variable

$$\xi = x - \beta_{\rm w}t, \tag{9}$$

where $\beta_{\rm w} = v_{\rm w}/c$ is the normalized phase velocity of the wake wave $v_{\rm w}$, allows us to obtain the time-independent Lagrangian for photons (i.e. for the short-wavelength electromagnetic wave packet):

$$\mathcal{L} = -\omega_{\rm pe}\left(\xi\right)\sqrt{1 - \left(\dot{\xi} + \beta_{\rm w}\right)^2}. \tag{10}$$

Differentiating this Lagrangian with respect to time and using the Euler–Lagrange equation

$$\frac{\mathrm{d}}{\mathrm{d}t}\left(\frac{\partial\mathcal{L}}{\partial\dot{\xi}}\right) - \frac{\partial\mathcal{L}}{\partial\xi} = 0, \tag{11}$$

we obtain

$$\frac{\mathrm{d}\mathcal{L}}{\mathrm{d}t} = \frac{\partial\mathcal{L}}{\partial t} + \frac{\partial\mathcal{L}}{\partial\xi}\dot{\xi} + \frac{\partial\mathcal{L}}{\partial\dot{\xi}}\ddot{\xi} = \frac{\partial\mathcal{L}}{\partial t} + \frac{\mathrm{d}}{\mathrm{d}t}\left(\frac{\partial\mathcal{L}}{\partial\dot{\xi}}\right)\dot{\xi} + \frac{\partial\mathcal{L}}{\partial\dot{\xi}}\ddot{\xi} = \frac{\partial\mathcal{L}}{\partial t} + \frac{\mathrm{d}}{\mathrm{d}t}\left(\frac{\partial\mathcal{L}}{\partial\dot{\xi}}\dot{\xi}\right). \tag{12}$$

In the case of the time-independent Lagrangian, $\partial\mathcal{L}/\partial t = 0$, this gives the Jacobi integral conservation:

$$\frac{\mathrm{d}}{\mathrm{d}t}\left(\frac{\partial\mathcal{L}}{\partial\dot{\xi}}\dot{\xi} - \mathcal{L}\right) = \frac{\mathrm{d}\mathcal{H}_{\rm O}}{\mathrm{d}t} = 0. \tag{13}$$

The Jacobi integral is equal to

$$\mathcal{H}_{\rm O}\left(\xi,\dot{\xi}\right) = \frac{\omega_{\rm pe}\left(\xi\right)\left(1 - \dot{\xi}\beta_{\rm w} - \beta_{\rm w}^2\right)}{\sqrt{1 - \left(\dot{\xi} + \beta_{\rm w}\right)^2}}. \tag{14}$$

In terms of the coordinate ξ and momentum

$$\frac{\partial \mathcal{L}}{\partial \dot{\xi}} = \frac{\omega_{\rm pe}^2 \left(\dot{\xi} + \beta_{\rm w}\right)}{\sqrt{1 - \left(\dot{\xi} + \beta_{\rm w}\right)^2}} = k, \tag{15}$$

it is equal to the Hamiltonian

$$\mathcal{H}_{\rm O}(\xi, k) = \sqrt{k^2 + \omega_{\rm pe}^2(\xi)} - \beta_{\rm w} k, \tag{16}$$

which results in the equations of motion

$$\dot{k} = -\partial_\xi \mathcal{H}_{\rm O} = -\frac{\omega_{\rm pe}}{\sqrt{k^2 + \omega_{\rm pe}^2(\xi)}} \partial_\xi \omega_{\rm pe} \quad \text{and} \quad \dot{\xi} = \partial_k \mathcal{H}_{\rm O} = \frac{k}{\sqrt{k^2 + \omega_{\rm pe}^2(\xi)}} - \beta_{\rm w}. \tag{17}$$

As we noticed above, time-independent Hamiltonian is an integral of motion (it is the Jacobi integral),

$$\mathcal{H}_{\rm O}(\xi, k) = h_{\rm O}, \tag{18}$$

where $h_{\rm O}$ is a constant. Using the relationship $k = \sqrt{\omega^2 - \omega_{\rm pe}^2(\xi)}$, we rewrite equation (18) as

$$\omega - \beta_{\rm w} \sqrt{\omega^2 - \omega_{\rm pe}^2(\xi)} = h_{\rm O}. \tag{19}$$

Its solution can be written in the form

$$\omega = \frac{h_{\rm O} \pm \beta_{\rm w} \sqrt{h_{\rm O}^2 - (1 - \beta_{\rm w}^2)\,\omega_{\rm pe}^2(\xi)}}{1 - \beta_{\rm w}^2}. \tag{20}$$

2.1.2. Phase plane

To find the maximum frequency upshift, we need to analyze the topology of the phase plane of the dynamical system (17). Contours corresponding to a constant value of the Hamiltonian $\mathcal{H}_{\rm O}(\xi, k)$ given by equation (16) are presented in figure 1(a) for a model dependence of the plasma frequency on the coordinate ξ,

$$\omega_{\rm pe}(\xi) = \omega_{\rm pe}(0) \left(\frac{1 + \delta \cos(k_{\rm w} \xi)}{1 + \delta} \right), \tag{21}$$

where $\beta_{\rm w} = 0.95$, $\omega_{\rm pe}(0) = 1$, $k_{\rm w} = 1$, and $\delta = 0.5$ (the case where the dependence of the plasma frequency on the coordinate ξ is given by a nonlinear wake wave was considered in [41]). Figure 1(b) shows iso-contours of the Jacobi integral given by equation (19).

As one can see, the trajectories of dynamical system described by equations (17) are either trapped or transient in the (ξ, k) plane. The domain of trapped trajectories is encircled by the separatrix whose branches intersect each other in the unstable point of equilibrium,

$$\xi = 2\pi n, \quad k = \beta_{\rm w} \frac{\omega_{\rm pe}(2\pi n)}{\sqrt{1 - \beta_{\rm w}^2}}, \tag{22}$$

with $n = 0, \pm 1, \pm 2, \ldots$, where the local group velocity of the electromagnetic wave packet is equal to the phase velocity of the wake wave. The frequency corresponding to the unstable critical point

$$\omega_{\rm X} = \frac{\omega_{\rm pe}(0)}{\sqrt{1 - \beta_{\rm w}^2}} \tag{23}$$

is marked in figure 1(b) by a horizontal dashed line.

The coordinates of stable points of equilibrium are

$$\xi = \pi(2m + 1), \quad k = \beta_{\rm w} \frac{\omega_{\rm pe} \pi (2m + 1)}{\sqrt{1 - \beta_{\rm w}^2}}, \tag{24}$$

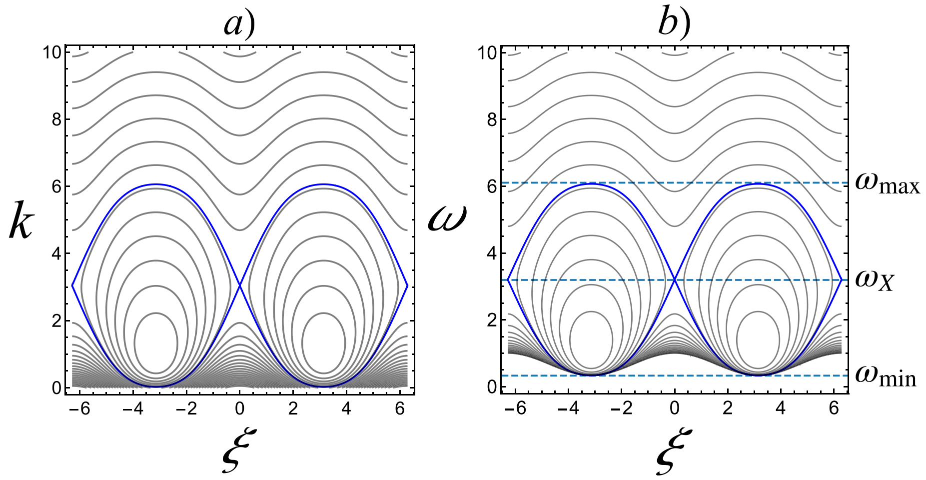

Figure 1. Contours of constant value of (a) the Hamiltonian $\mathcal{H}_{\rm O}(\xi, k)$ given by equation (16) and (b) the Jacobi integral $\mathcal{H}_{\rm O}(\xi,\omega)$ given by equation (19) for $\beta_{\rm w}=0.95$, $\omega_{\rm pe}(0)=1$, $k_{\rm w}=1$, and $\delta=0.5$. Here $\omega_{\min}$ and $\omega_{\max}$ are, respectively, the minimum and maximum frequencies on the separatrix whose critical point is $(0, \omega_{\rm X})$.

with $m=0,\pm1,\pm2,\ldots$. On the separatrix, the constant on the right-hand side (r.h.s.) of equation (18) equals

$$h=\omega_{\rm pe}(0)\sqrt{1-\beta_{\rm w}^2}. \tag{25}$$

The phase plane (ξ,ω) shown in figure 1(b) is similar to the (ξ,k) plane with the separatrix determined by the constant in the r.h.s. of equation (19) also equal to $h=\omega_{\rm pe}(0)\sqrt{1-\beta_{\rm w}^2}$. The coordinates of the critical points on the separatrix in the (ξ,ω) plane are $\xi=\pi n$ and $\omega=\omega_{\rm pe}(\pi n)/\sqrt{1-\beta_{\rm w}^2}$.

The maximum frequency upshift, which is equal to the difference between the maximum and minimum values of the electromagnetic pulse frequency on the trajectory, is reached when the trajectory is the separatrix, i.e. the first integral is equal to $h_{\rm O}=\omega_{\rm pe}(0)\sqrt{1-\beta_{\rm w}^2}$. Substituting it into equation (20) we obtain the maximum and minimum of the electromagnetic pulse frequency on the separatrix

$$\omega_{\max,\min}=\frac{\omega_{\rm pe}(0)\pm\beta_{\rm w}\sqrt{\omega_{\rm pe}^2(0)-\omega_{\rm pe}^2(\pi)}}{\sqrt{1-\beta_{\rm w}^2}}, \tag{26}$$

corresponding to plus and minus sign in the r.h.s. of this equation, i.e. the maximum upshift of frequency is

$$\Delta\omega_{\max}=\frac{2\beta_{\rm w}\sqrt{\omega_{\rm pe}^2(0)-\omega_{\rm pe}^2(\pi)}}{\sqrt{1-\beta_{\rm w}^2}}. \tag{27}$$

For $\beta_{\rm w}\to1$ and $\omega_{\rm pe}^2(0)\gg\omega_{\rm pe}^2(\pi/2)$, it is approximately equal to $\omega_{\max}\approx2\omega_{\rm pe}(0)\gamma_{\rm w}$, where the gamma factor equals

$$\gamma_{\rm w}=\frac{1}{\sqrt{1-\beta_{\rm w}^2}}, \tag{28}$$

i.e. it formally follows from equation (27) that the upshifted frequency tends to infinity at $\beta_{\rm w}\to1$. The minimum frequency, which can be considered as a wave frequency before interaction with the wake wave or the frequency of the electromagnetic pulse 'injected' in the accelerating phase of the photon accelerator, is

$$\omega_{\min}\approx\omega_{\rm pe}(0)\sqrt{\frac{1-\beta_{\rm w}}{1+\beta_{\rm w}}}\approx\frac{\omega_{\rm pe}(0)}{2\gamma_{\rm w}}, \tag{29}$$

as follows from equation (20) for $h_{\rm O}=\omega_{\rm pe}(0)\sqrt{1-\beta_{\rm w}^2}$. If it is expressed in terms of the frequency $\omega_0=\omega_{\min}$, the maximum upshifted frequency can be written as $\omega_m\approx4\gamma_{\rm w}\omega_0$ for $\omega_0=\omega_{\min}$, which is similar to the frequency upshift obtained in the case of a relativistic flying mirror [21, 43]. By virtue of the Lorentz invariance of the ratio of the electric field of the wave to the frequency of the wave, the amplitude of the electromagnetic wave packet also increases proportionally to $4\gamma_w^2$.

For a given frequency ω_0 to be approximately equal $\omega_{\min}$, the modulation of the refractive index must be large enough, which leads to the requirement that $\omega_{pe}(0) \geq 2\omega_0\gamma_w^2$, otherwise the trajectory of the electromagnetic wave packet will not be located inside the region bounded by the separatrix. Unlike the case of relativistic flying mirrors, within the framework of the 'photon accelerator' concept based on the geometric optics approximation, the frequency shift of an electromagnetic pulse propagating along a trajectory significantly above or below the separatrix wave on a plane is relatively small, since the reflection coefficient of the electromagnetic wave from the wake crest in this case is zero. Another fundamentally important difference between a photon accelerator and a relativistic plasma mirror is that in the case of a photon accelerator, the accelerated electromagnetic pulse propagates in the same direction as the modulation of the refractive index [see figure 1(b), where the wave number is always positive], whereas in the case of a relativistic mirror, it can collide with the mirror head-on, which provides a large frequency shift (see also the discussion in references [44–47]).

Here, we have analyzed the properties of a photon accelerator in one-dimensional (1D) geometry assuming homogeneous unmagnetized plasma. These two assumptions significantly simplify the analysis of the problem, making it possible to provide a clear analytical characterization. In general case, the photon acceleration is a three-dimensional (3D) process happening in inhomogeneous plasma. However, the analysis of this process is beyond the scope of the present work. We note that in the case of relativistic mirrors there are several papers on the multi-dimensional analysis of these phenomena taking place in different plasma environments. For example, 3D effects significantly modify the properties of electromagnetic wave interactions with electron density modulations. The focusing of a laser pulse by a paraboloidal wake wave [48, 49] leads to a scaling of upshifted frequency with group velocity different from the 1D case [50–53]. Other spatial and temporal shapes of electron density modulations can be considered to optimize the reflection and intensification efficiencies as shown in [21, 43, 44, 50]. The plasma density inhomogeneity, on the other hand, can result in the dephasingless regime of the photon acceleration (see [7–9, 54]). The photon accelerator can be also driven by the electron/proton beams [55, 56].

We note that the symmetry of the interaction of an electromagnetic wave and a plasma wave, when dependence of the refraction index on time and coordinate has the form given by equation (21), $\xi = x - \beta_w t$, leads to the conservation of the Jacobi integral

$$\omega - \beta_w k = h. \tag{30}$$

2.2. Extraordinary electromagnetic wave

For the extraordinary wave (it is also called the X-wave) the relationship between the wave frequency and wave number has a form (see, e.g. [57])

$$\frac{k^2}{\omega^2} = 1 - \frac{\omega_{pe}^2\left(\omega^2 - \omega_{pe}^2\right)}{\omega^2\left(\omega^2 - \omega_{pe}^2 - \omega_{Be}^2\right)}, \tag{31}$$

where $\omega_{Be} = eB/m_e c$ is the electron Larmor frequency and B denotes the magnetic field. In the normalized form the electron Larmor frequency can be written as

$$\omega_{Be} = \frac{eB}{k_w m_e c^2}. \tag{32}$$

If the wave frequency becomes equal to

$$\omega = \omega_{UH} = \sqrt{\omega_{pe}^2 + \omega_{Be}^2} \tag{33}$$

the denominator in the r.h.s. of equation (31) tends to zero, which corresponds to the upper hybrid (UH) resonance. The ion component is assumed to be at rest. The electromagnetic wave can propagate provided that the square of the wave number is positive, i.e. in frequency ranges

$$\omega_1 < \omega < \omega_{UH} \quad \text{and} \quad \omega_2 < \omega, \tag{34}$$

where

$$\omega_{1,2} = \sqrt{\frac{\omega_{pe}^2 + \omega_{UH}^2}{2} \pm \sqrt{\frac{\left(\omega_{pe}^2 + \omega_{UH}^2\right)^2}{4} - \omega_{pe}^4}}. \tag{35}$$

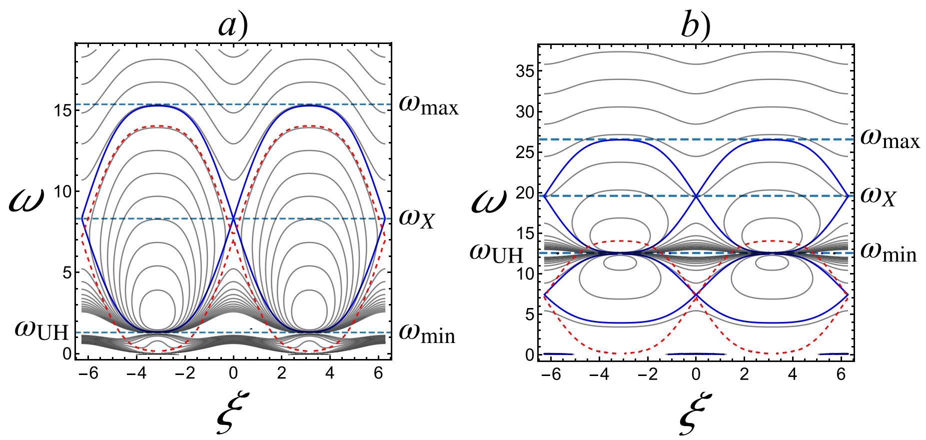

Figure 2. Contours of constant value of the integral $\mathcal{H}_X(\xi,\omega)$ given by equation (36) for the X-wave. Here $\beta_w = 0.999$, $\omega_{pe}(0) = 1$, the refraction index modulation amplitude is determined by $\delta = 0.5$, and Larmor frequency is equal to $\omega_{Be} = 1.25$ in frame (a) and $\omega_{Be} = 12.5$ in frame (b). As in figure 1, $\omega_{\min}$ and $\omega_{\max}$ are, respectively, the minimum and maximum frequencies on the separatrix (blue curve) whose critical point is $(0,\omega_X)$. Red dashed curves show the separatrices for $\omega_{Be} = 0$.

Equations of motion of a short electromagnetic wave (X-wave) packet within the framework of geometric optics approximation have the Jacobi integral

$$\mathcal{H}_X(\xi,\omega) = \omega - \beta_w \sqrt{\omega^2 - \omega_{pe}^2(\xi)\,\frac{\omega^2 - \omega_{pe}^2(\xi)}{\omega^2 - \omega_{UH}^2(\xi)}} = h_X. \tag{36}$$

For the Jacobi integral $\mathcal{H}_X(\xi,\omega)$ of the X-wave given by equation (36), the phase plot is presented in figure 2 with the following parameters: the normalized phase velocity of the refraction index modulations is $\beta_w = 0.999$, the Langmuir frequency at the maximum is $\omega_{pe}(0) = 1$, the amplitude of the modulations of refraction index is given by equation (21) with the refraction index modulation amplitude determined by $\delta = 0.5$, and the Larmor frequency is equal to $\omega_{Be} = 1.25$ in frame a) and $\omega_{Be} = 12.5$ in frame b). As in figure 1, $\omega_{\min}$ and $\omega_{\max}$ are, respectively, the minimum and maximum frequencies on the separatrix whose critical point is $(0,\omega_X)$. Red dashed curves show the separatrices for $\omega_{Be} = 0$.

As shown in figures 2(a) and (b), the stripe around the UH frequency ω_{UH}, i.e. in the region of the UH resonance, subdivides the phase plane in two subdomains. A strong magnetic field ($\omega_{Be} \gg \omega_{pe}$) ensures effective interaction of the electromagnetic pulse with the wake wave, enabling a significantly higher maximum upshifted frequency compared to the case of weakly magnetized plasma. Within a narrow stripe in the vicinity of the UH resonance region, the X-wave decays via generation of the electrostatic Bernstein wave and subsequent electron heating. We leave this regime discussion to forthcoming papers.

3. Photon acceleration for circularly polarized electromagnetic waves propagating along a magnetic field

In this section, we consider circularly polarized electromagnetic waves propagating in plasmas in the presence of a strong magnetic field with the goal to demonstrate the difference between the L- and R-wave polarizations (left- or right-rotated electric field). The R-wave corresponds to right-handed circular polarization with the electric field rotating in the same sense as electron gyration. In the L-wave the electric field rotates in the opposite direction. The dispersion equation gives the relationship between the wave number and wave frequency for circularly polarized electromagnetic waves propagating along the magnetic field B (see [57]):

$$\frac{k^2}{\omega^2} = 1 - \frac{\omega_{pe}^2}{\omega(\omega \pm \omega_{Be})}. \tag{37}$$

The ion component is assumed to be at rest. The plus and minus signs in the r.h.s. correspond to the left circularly polarized wave (or an L-wave) and to the right circularly polarized wave (or an R-wave), respectively. The latter is often referred to as the whistler mode. The electromagnetic wave can propagate

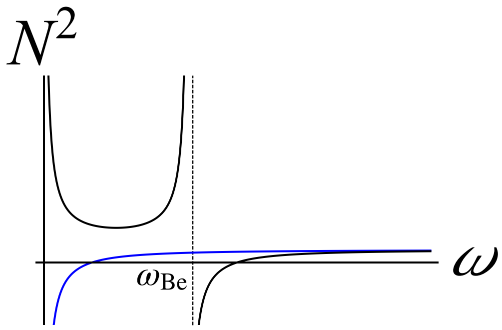

Figure 3. Square of refraction index for R- and L-waves (black and blue curves, respectively) given by equation (37) as a function of the wave frequency ω for $\omega_{\rm pe}(0) = 1$ and $\omega_{\rm Be} = 1.5$. The waves can propagate in the region of parameters where $N^2 > 0$.

provided that the square of the wave number is positive, i.e. its frequency is bounded by the following limits

$$0 < \omega < \omega_{\rm Be} \quad \text{and} \quad \omega > \frac{1}{2}\sqrt{\omega_{\rm Be}^2 + 4\omega_{\rm pe}^2(\xi)} + \omega_{\rm Be} \tag{38}$$

for the R-wave, and

$$\omega > \frac{1}{2}\sqrt{\omega_{\rm Be}^2 + 4\omega_{\rm pe}^2(\xi)} - \omega_{\rm Be} \tag{39}$$

for the L-wave. As we can see, the denominator in r.h.s. of equation (37) vanishes for R-wave when the wave frequency becomes equal to the Larmor frequency. This corresponds to the cyclotron resonance between the electron Larmor rotation and the electromagnetic wave. In figure 3, we present the square of the refraction index $N^2 = k^2/\omega^2$ for R- and L-waves (black and blue curves, respectively) given by equation (37) as a function of the wave frequency ω for $\omega_{\rm pe} = 1$ and $\omega_{\rm Be} = 1.5$. As it was mentioned above, the condition for the electromagnetic wave to be able to propagate in plasmas is that the square of the wave number is positive, or $N^2 > 0$.

From the dispersion equation (37), we can find the dependence of the wave frequency on the wave number. However, since equation (37) is cubic algebraic equation of the third order, it is cumbersome and it is therefore convenient to analyze the (ξ, ω) phase space using the Jacobi integral $\mathcal{H}_{\rm R}(\xi,\omega) = h_{\rm R}$ written in the form

$$\mathcal{H}_{\rm R}(\xi,\omega) = \omega - \beta_{\rm w}\sqrt{\omega^2 - \frac{\omega\omega_{\rm pe}^2(\xi)}{\omega - \omega_{\rm Be}}} = h_{\rm R} \tag{40}$$

for the R-wave, and

$$\mathcal{H}_{\rm L}(\xi,\omega) = \omega - \beta_{\rm w}\sqrt{\omega^2 - \frac{\omega\omega_{\rm pe}^2(\xi)}{\omega + \omega_{\rm Be}}} = h_{\rm L} \tag{41}$$

for the L-wave, respectively.

Using dispersion equation (41), we can derive the expression for the group velocity of the R- and L-waves, $v_{\rm g} = \partial_k \omega$. It is

$$v_{\rm g}(\omega,\xi) = \frac{2(\omega \pm \omega_{\rm Be})^2\sqrt{\omega^2 - \omega\omega_{\rm pe}^2(\xi)/(\omega \pm \omega_{\rm Be})}}{2\omega(\omega \pm \omega_{\rm Be})^2 \mp \omega_{\rm Be}\omega_{\rm pe}^2(\xi)}, \tag{42}$$

where the plus sign corresponds to the L-wave and the minus sign corresponds to the R-wave. The group velocity vanishes at the points given by equations (38) and (39) [see figure 4, where group velocities defined by equation (42) are shown for $\omega_{\rm pe}(0) = 1$].

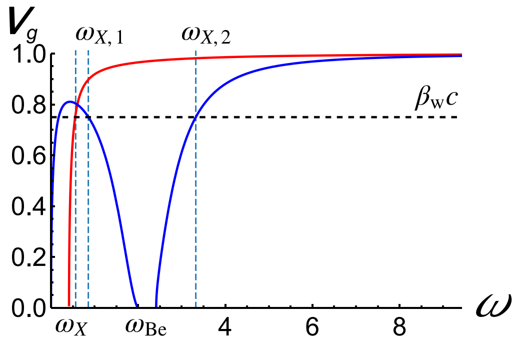

Figure 4. Group velocity of electromagnetic pulse (red color curve for L-wave and blue color curve for R-wave) versus the wave frequency at $\omega_{pe} = \omega_{pe}(0)$. The points, where the group velocity is equal to the phase velocity of the refraction index modulation, $\beta_w c$, correspond to the critical points on the separatrix ω_X, or $\omega_{X,1}$, and $\omega_{X,2}$, where two separatrix branches intersect each other. Here $\beta_w = 0.75$, $\omega_{pe}(0) = 1$, and $\omega_{Be} = 2$.

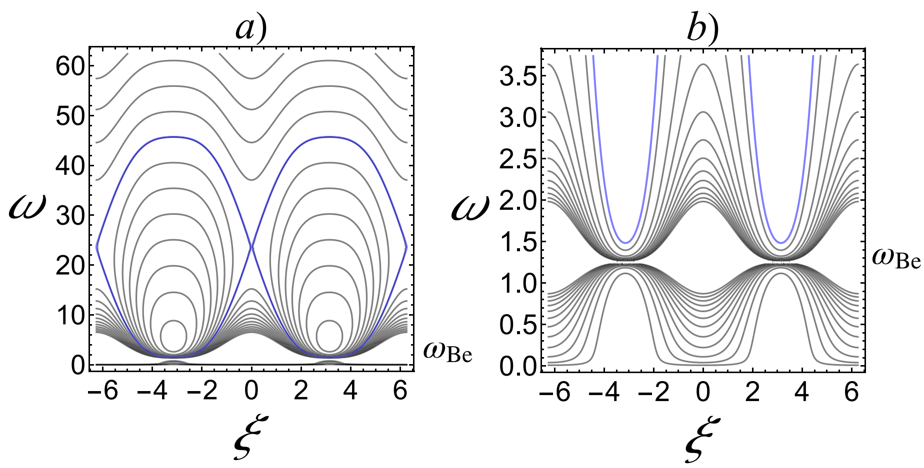

Figure 5. (a) Contours of constant value of the Jacobi integral $\mathcal{H}_R(\xi,\omega)$ given by equation (40) for $\beta_w = 0.999$, $\omega_{pe}(0) = 1$, $\omega_{Be} = 1.25$, and $\delta = 0.75$; (b) zoom of the region near $\omega = \omega_{Be}$. Blue curves stand for the separatrix trajectories.

3.1. R-wave

Contours of constant value of the integral $\mathcal{H}_R(\xi,\omega)$ given by equation (40) for the R-wave in the case when Langmuir frequency is approximately equal to Larmor frequency, $\omega_{pe} \approx \omega_{Be}$, are presented in figure 5(a) for $\beta_w = 0.999$, $\omega_{pe} = 1$, $\omega_{Be} = 1.25$, and $\delta = 0.75$. Figure 5(b) shows a zoom of the region near $\omega = \omega_{Be}$.

The stripe near the Larmor frequency where $\omega = \omega_{Be}$ [ω_{Be} is determined by equation (32)] subdivides the phase plane into two subdomains $\omega < \omega_{Be}$ and $\omega > \omega_{Be}$. If the electromagnetic pulse is injected into the photon accelerator with the frequency $\omega \ll \omega_{Be}$, its frequency upshift is limited by the value equal to the Larmor frequency: $\omega_m \leq \omega_{Be}$. In the case the wave packet is injected into the photon accelerator with the frequency $\omega \approx \omega_{Be}$, the maximum frequency upshift is achieved when the packet trajectory is the separatrix [it is a blue curve in the plane (ξ,ω)]. Since in the limit $\beta_w \to 1$ the electromagnetic wave frequency is well above that, we can find the coordinates of the point of the separatrix branch crossing, assuming smallness of the ratio ω_{Be}/ω, as

$$\xi_x = 2\pi n, \quad \omega_{X,R/L} \approx \frac{\omega_{pe}(\pi n)}{\sqrt{1-\beta_w^2}} \pm \frac{1+\beta_w^2}{2}\omega_{Be}. \tag{43}$$

The point, where the group velocity is equal to the phase velocity of the refraction index modulation (it is $\beta_w c$), corresponds to the critical point on the separatrix ω_X, where two separatrix branches intersect each other. Substituting this expression into the first integral determined by equation (40), we find that the constant h_R for upper critical point (where $\omega_{X,2} > \omega_{Be}$) is equal to

$$h_{R,L} \approx \omega_{pe}(0)\sqrt{1-\beta_w^2} \pm \frac{1-\beta_w^2}{2}\omega_{Be}. \tag{44}$$

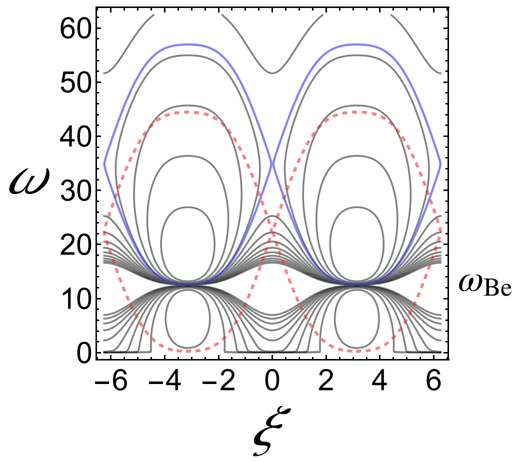

Figure 6. Contours of constant value of Jacobi integral $\mathcal{H}_{\mathrm{R}}(\xi,\omega)$ given by equation (40) for the Larmor frequency substantially larger than the Langmuir frequency for $\beta_{\mathrm{w}} = 0.999$, $\omega_{\mathrm{pe}}(0) = 1$, $\omega_{\mathrm{Be}} = 12.5$, and $\delta = 0.75$. The red dashed curve shows the separatrix for $\omega_{\mathrm{Be}} = 0$.

Using this and equations (45)–(46), we can obtain the maximum value of upshifted frequency, which corresponds to the frequency on the top point of the separatrix on the (ξ,ω) plane. It is

$$\omega_{\max} \approx \frac{h_{\mathrm{R,L}}}{1-\beta_{\mathrm{w}}} = \omega_{\mathrm{pe}}(0)\sqrt{\frac{1+\beta_{\mathrm{w}}}{1-\beta_{\mathrm{w}}}} \pm \frac{1+\beta_{\mathrm{w}}}{2}\omega_{\mathrm{Be}}. \tag{45}$$

Minimum frequency is approximately equal to the Larmor frequency, $\omega_{\min} \approx \omega_{\mathrm{Be}}$.

In the lower subdomain on the phase plane, where $\omega < \omega_{\mathrm{Be}}$, the minimum frequency here is approximately equal to zero as we can also see in figure 5 while the maximum frequency equals the Larmor frequency, $\omega_{\max} \approx \omega_{\mathrm{Be}}$. Thus, for the electromagnetic pulse to reach the maximum upshifted frequency, its initial frequency should be above the value of the cutoff frequency determined by equation (38),

$$\frac{1}{2}\sqrt{\omega_{\mathrm{Be}}^2 + 4\omega_{\mathrm{pe}}^2(\xi)} + \omega_{\mathrm{Be}}, \tag{46}$$

otherwise it will end up with the frequency that is below the Larmor frequency.

In figure 6, we present the phase plane of the Jacobi integral $\mathcal{H}_{\mathrm{R}}(\xi,\omega)$ given by equation (40) for a Larmor frequency that is substantially larger than the Langmuir frequency for $\beta_{\mathrm{w}} = 0.999$, $\omega_{\mathrm{pe}}(0) = 1$, $\omega_{\mathrm{Be}} = 12.5$, and $\delta = 0.75$. For comparison with the case of zero magnetic field, we plot a red dashed separatrix curve for the same parameters, but zero magnetic field. It is seen that the magnetic field effects result in significant change to the upshifted frequency of the R-wave.

3.2. L-wave

The phase plot of the Jacobi integral $\mathcal{H}_{\mathrm{L}}(\xi,\omega)$ determined by equation (41) for the L-wave is shown in figure 7. Here the Langmuir frequency is substantially smaller than the Larmor frequency, $\omega_{\mathrm{pe}} \ll \omega_{\mathrm{Be}}$. The following parameters are being used: the normalized phase velocity of the refraction index modulations is $\beta_{\mathrm{w}} = 0.999$, the Langmuir frequency at the maximum is $\omega_{\mathrm{pe}}(0) = 1$, the Larmor frequency equals to $\omega_{\mathrm{Be}} = 2.5$, and the amplitude of the modulations of refraction index is given by equation (21) with the refraction index modulation amplitude determined by $\delta = 0.15$ in frame a) and $\delta = 0.75$ in frame b). As in figure 1, $\omega_{\min}$ and $\omega_{\max}$ are, respectively, the minimum and maximum frequencies on the separatrix whose critical point is $(0,\omega_{\mathrm{X}})$.

To find the coordinates of the critical point of the separatrix trajectory on the phase plane (ξ,ω), where two separatrix branches intersect each other, assuming $\omega_{\mathrm{pe}} \ll \omega_{\mathrm{Be}}$, we calculate the group velocity of the electromagnetic pulse,

$$v_{\mathrm{g}}(\omega,\xi) \approx c\left(1 - \frac{\omega_{\mathrm{pe}}^2(\xi)}{2(\omega+\omega_{\mathrm{Be}})^2}\right). \tag{47}$$

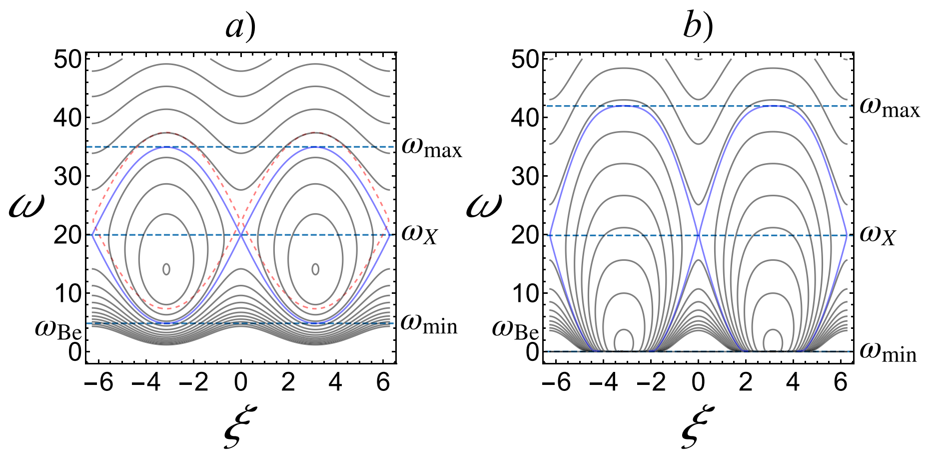

Figure 7. Contours of constant value of the Jacobi integral $\mathcal{H}_{\mathrm{L}}(\xi,\omega)$ given by equation (41) for $\beta_{\mathrm{w}}=0.999$, $\omega_{\mathrm{pe}}(0)=1$, $\omega_{\mathrm{Be}}=2.5$, and the refraction index modulation amplitude is determined by $\delta=0.15$ in frame (a) and $\delta=0.75$ in frame (b). Here, as in figure 1, $\omega_{\min}$ and $\omega_{\max}$ are, respectively, the minimum and maximum frequencies on the separatrix (blue curve) whose critical point is $(0,\omega_{\mathrm{X}})$. Red dashed curve in frame (a) shows the separatrix for $\omega_{\mathrm{Be}}=0$.

At the point $(0,\omega_{\mathrm{X}})$, the group velocity equals the phase velocity of the refraction index modulations, $c\beta_{\mathrm{w}}$, which gives

$$\omega_{\mathrm{X}}=\frac{\omega_{\mathrm{pe}}(0)}{\sqrt{2(1-\beta_{\mathrm{w}})}}-\omega_{\mathrm{Be}}. \tag{48}$$

The value of the Jacobi integral on the separatrix trajectory is

$$h_{\mathrm{X}}=\frac{\omega_{\mathrm{pe}}(0)}{\sqrt{2}}\sqrt{1-\beta_{\mathrm{w}}}-\omega_{\mathrm{Be}}(1-\beta_{\mathrm{w}}). \tag{49}$$

As a result, we obtain for the maximum and minimum frequencies

$$\omega_{\max/\min}=\frac{\omega_{\mathrm{pe}}(0)\pm\sqrt{\omega_{\mathrm{pe}}^2(0)-4\beta_{\mathrm{w}}\omega_{\mathrm{pe}}^2(\xi_{\min/\max})}}{2^{3/2}\sqrt{1-\beta_{\mathrm{w}}}}-\omega_{\mathrm{Be}}. \tag{50}$$

Here $\xi_{\min}$ is the coordinate where the electromagnetic pulse frequency is at a minimum. In the case of a sufficiently small modulation amplitude, i.e. for $\omega_{\mathrm{pe}}^2(0)>4\beta_{\mathrm{w}}\omega_{\mathrm{pe}}^2(\pi/2)$, the minimum and maximum frequency values $\omega_{\max/\min}$ are given by equation (50) with $\xi_{\min/\max}=\pi/2k_{\mathrm{w}}$. This case is illustrated by figure 7(a). If $\omega_{\mathrm{pe}}^2(0)<4\beta_{\mathrm{w}}\omega_{\mathrm{pe}}^2(\pi/2)$, the minimum frequency equals

$$\omega_{\min}=\frac{\omega_{\mathrm{pe}}(0)}{2^{3/2}\sqrt{1-\beta_{\mathrm{w}}}}-\omega_{\mathrm{Be}}. \tag{51}$$

For comparison with the case of zero magnetic field, we show in figure 7(a) by a red dashed curve a separatrix for the same parameters, but zero magnetic field. It is seen that the magnetic field effects do not lead to significant change of the upshifted frequency of the L-wave.

4. Conclusion and discussion

Theoretical consideration and experimental implementation of the effects of strong magnetic fields in laser accelerators of charged particles and photons open new directions in the development of an understanding of active processes in space active objects and the application of the acquired knowledge in materials science, biology, and fundamental sciences. It was shown that a magnetic field changes the electromagnetic wave interactions with the relativistic plasma wave, it could also lead to an achievable frequency increase within the photon accelerator paradigm.

As noted above, the frequency of the wave packet shifts toward higher frequencies by a factor proportional to the square of the gamma factor corresponding to the velocity of modulation of the refractive index, and due to the Lorentz invariance of the ratio of the electric field of the wave to the frequency of the wave, the amplitude of the electromagnetic wave packet also increases in proportion to the same factor.

The length over which the maximum frequency upshift is reached (it can be called 'the photon acceleration length') is approximately equal to

$$l_{\mathrm{acc}} \approx \frac{2\pi k_{\mathrm{w}}^{-1}}{1-\beta_{\mathrm{w}}}. \tag{52}$$

The effects of a magnetic field lead to quantitative and qualitative changes in the properties of photon acceleration, opening novel opportunities for optimization and increased efficiency. As expected, the most pronounced effect of a magnetic field occurs during the interaction of extraordinary electromagnetic waves with refractive index modulations moving at relativistic phase velocity which can be generated in a plasma embedded in the static magnetic field in a wake of the driver short pulse laser. Considered above extraordinary electromagnetic waves are the right circularly polarized waves propagating along the static magnetic field in the electron–ion plasma, and the X-wave propagating across the magnetic field. It should be noted that the configuration corresponding to the interaction of high-intensity X-wave with a solid target has shown extremely high efficiency in generating gamma-ray bursts [58]. It has also attracted active attention in connection with the development of the theory of charged particle acceleration and radiation emission from pulsars and magnetars [59].

To demonstrate high electromagnetic wave frequency upshifts, ultrastrong magnetic field will require strengths well above the magnetic field achievable with static and pulsed magnets. The self-generated fields in relativistic laser plasma (see, e.g. [55, 60–66] and literature cited therein) are one of candidates. With future advances, coil targets may also be a promising source of strong magnetic fields [67–70]. In laser plasma interactions with near-critical electron density targets (the critical electron density $n_{\mathrm{cr}} = m_{\mathrm{e}}\omega^2/4\pi e^2$ for one-micron wavelength laser is equal to $\approx 1.2 \times 10^{21}$ cm^{-3}) the Larmor and the Langmuir frequencies are equal to each other for the magnetic field strength of 0.1 GG. We note that in theoretical/computer simulation publications [67–70] the magnetic field strength is found to reach 10 GG. Laboratory measurements of magnetic fields generated during high-intensity laser interactions with dense plasmas [70] showed the generation of magnetic fields with a strength of 0.7 GG localized in a small region with high density near the front surface of solid target. In an extended plasma the magnetic field generated by coil target reached 0.6 kT (i.e. 600 MG) as reported in [66]. As we see, in laser plasma the effects of self-generated magnetic field [71] and magnetic field created with coil-like targets [67–70] can significantly modify the photon accelerator scenario compared with the case of unmagnetized plasma.

We also note that the theory of photon acceleration employed above is formulated within the framework of the geometric optics approximation, which describes either complete reflection or complete transmission of the wave (see, e.g. [36, 37]). Frequency upshifting and wave intensification can also be realized when relativistic plasma mirrors are formed by nonlinear plasma waves, whose breaking leads to the formation of singular electron-density structures enabling partial reflection of electromagnetic waves, as proposed in [21]. The theory developed there relies on approaches that go beyond the geometric optics approximation. For further details, see the reviews [51, 72].

As is well known, strong absorption of electromagnetic waves occurs in the vicinity of the UH and cyclotron resonances (see, e.g. the discussion of these effects in ionospheric plasma in [73] and references therein). Revealing these effects in relativistic collisionless plasma requires multi-parametric computer simulations, as in the study reported in [58], which is devoted to the influence of ultrastrong magnetic fields on laser-produced gamma-ray flashes.

Acknowledgment

The authors thank Tales Augusto Oliveira Gomes, Prokopis Hadjisolomou, Tae Moon Jeong, and Rashid Shaisultanov for fruitful discussions.

Data availability statement

All data that support the findings of this study are included within the article (and any supplementary files).

Funding

SSB was supported by U.S. Department of Energy Office of Science Office of High Energy Physics under Contract No. DE-AC02-05CH11231. AGRT was supported by the U.S. National Science Foundation Award No. 2512 014. PV was supported by the Ministry of Education, Youth and Sports of the Czech Republic through the e-INFRA CZ (ID:90254).

ORCID iDs

S V Bulanov 0000-0001-8305-0289
S S Bulanov 0000-0002-9861-9391
T Z Esirkepov 0000-0002-9027-0703
G Gregori 0000-0002-4153-0628
G M Grittani 0000-0003-4394-854X
M Lamač 0000-0001-9218-6073
B K Russell 0000-0003-0011-2419
A G R Thomas 0000-0003-3206-8512
P Valenta 0000-0003-1067-3762

References

[1] Wilks S C, Dawson J M, Mori W B, Katsouleas T and Jones M E 1989 Photon accelerator *Phys. Rev. Lett.* **62** 2600–3
[2] Mendonca J T 2000 *Theory of Photon Acceleration* (CRC Press)
[3] Mironov V A, Sergeev A M, Vanin E V, Brodin G and Lundberg J 1992 Upper limits for frequency up-conversion in the nonlinear photon accelerator *Phys. Rev. A* **46** R6178–80
[4] Bulanov S V, Esirkepov T Z, Kando M, Koga J K, Hosokai T, Zhidkov A G and Kodama R 2013 Nonlinear plasma wave in magnetized plasmas *Phys. Plasmas* **20** 83113
[5] Dias J M, Stenz C, Lopes N, Badiche X, Blasco F, Santos A D, Oliveirae L Mysyrowicz S A, Antonetti A and Mendonça J T 1997 Experimental evidence of photon acceleration of ultrashort laser pulses in relativistic ionization fronts *Phys. Rev. Lett.* **78** 4773–6
[6] Murphy C D *et al* 2006 Evidence of photon acceleration by laser wake fields *Phys. Plasmas* **13** 033108
[7] Sandberg R T and Thomas A G R 2023 Photon acceleration from optical to XUV *Phys. Rev. Lett.* **130** 085001
[8] Sandberg R T and Thomas A G R 2023 Electron-beam-driven plasma wakefield acceleration of photons *Phys. Plasmas* **30** 113105
[9] Sandberg R T and Thomas A G R 2024 Dephasingless plasma wakefield photon acceleration *Phys. Rev. E* **109** 025210
[10] Gonoskov A, Blackburn T G, Marklund M and Bulanov S S 2022 Charged particle motion and radiation in strong electromagnetic fields *Rev. Mod. Phys.* **94** 045001
[11] Russell B K et al 2025 Reaching extreme fields in laser-electron beam collisions with XUV laser light (arXiv:2506.01727)
[12] Tajima T and Dawson J M 1979 Laser electron accelerator *Phys. Rev. Lett.* **43** 267–70
[13] Esarey E, Schroeder C B and Leemans W P 2009 Physics of laser-driven plasma-based electron accelerators *Rev. Mod. Phys.* **81** 1229–85
[14] Tajima T and Malka V 2020 Laser plasma accelerators *Plasma Phys. Control. Fusion* **62** 034004
[15] Kato Y, Ebisuzaki T and Tajima T 2022 Wakefield acceleration in a jet from a neutrino-driven accretion flow around a black hole *Astrophys. J.* **929** 42
[16] Picksley A *et al* 2024 Matched guiding and controlled injection in dark-current-free, 10-GeV-class, channel-guided laser-plasma accelerators *Phys. Rev. Lett.* **133** 255001
[17] Lazzarini C M *et al* 2024 Ultrarelativistic electron beams accelerated by terawatt scalable kHz laser *Phys. Plasmas* **31** 030703
[18] Chen P, Tajima T and Takahashi Y 2002 Plasma wakefield acceleration for ultrahigh-energy cosmic rays *Phys. Rev. Lett.* **89** 161101
[19] Tajima T, Yan X Q and Ebisuzaki T 2020 Wakefield acceleration *Rev. Mod. Plasma Phys.* **4** 7
[20] Ebisuzaki T, Tajima T and Barish B C 2023 Wakefield acceleration in the universe *Int. J. Mod. Phys. D* **32** 2330001
[21] Bulanov S V, Esirkepov T Z and Tajima T 2003 Light Intensification towards the schwinger limit *Phys. Rev. Lett.* **91** 085001
[22] Colgate S A and Noerdlinger P D 1971 Coherent emission from expanding supernova shells *Astrophys. J.* **165** 509
[23] Yalinewich A and Pen U-L 2022 The moving mirror model for fast radio bursts *Mon. Not. R. Astron. Soc.* **515** 5682–8
[24] Lorimer D R, Bailes M, McLaughlin M A, Narkevic D J and Crawford F 2007 A bright millisecond radio burst of extragalactic origin *Science* **318** 777–80
[25] Petroff E, Hessels J W T and Lorimer D R 2022 Fast radio bursts at the dawn of the 2020s *Astron. Astrophys. Rev.* **30** 2
[26] Zhang B 2023 The physics of fast radio bursts *Rev. Mod. Phys.* **95** 035005
[27] Rees M J 1977 A better way of searching for black-hole explosions? *Nature* **266** 333–4
[28] Blandford R D 1977 Spectrum of a radio pulse from an exploding black hole *Mon. Not. R. Astron. Soc.* **181** 489–98
[29] Zweibel E G and Heiles C 1997 Magnetic fields in galaxies and beyond *Nature* **385** 131–6
[30] Harding A K and Lai D 2006 Physics of strongly magnetized neutron stars *Rep. Prog. Phys.* **69** 2631
[31] Askar'yan G A, Bulanov S V, Pegoraro F and Pukhov A M 1994 Magnetic interaction of self-focusing channels and fluxes of electromagnetic radiation: Their coalescence, the accumulation of energy and the effect of external magnetic fields on them *Sov. J. Exp. Theor. Phys. Lett.* **60** 251–7
[32] Amit M S Lad D, Mandal D, Jana K, Sarkar D, Das A and Kumar G R 2026 Tracking the complete evolution of electromagnetic instability in an ultra-intense laser-driven plasma *Matter Radiat. Extremes* **11** 027202
[33] Hosokai T, Kinoshita K, Zhidkov A, Maekawa A, Yamazaki A and Uesaka M 2006 Effect of external static magnetic field on the emittance and total charge of electron beams generated by laser-wakefield acceleration *Phys. Rev. Lett.* **97** 075004

[34] Eliezer S, Mendonça J T, Bingham R and Norreys P 2005 A new diagnostic for very high magnetic fields in expanding plasmas *Phys. Lett. A* **336** 390–5
[35] Whitham G B 2011 *Linear and Nonlinear Waves* (Wiley)
[36] Kravtsov Y A A and Orlov Y I 1990 *Geometrical Optics of Inhomogeneous Media* (Springer)
[37] Kaufman A N and Cohen B I 2019 Theoretical plasma physics *J. Plasma Phys.* **85** 205850601
[38] Dodin I Y, Lopez N A, Xing ngjing, Højlund Marholt R, and V H 2025 Geometrical optics in phase space (arXiv:2509.08098)
[39] Ginzburg V L 1962 *Propagation of Electromagnetic Waves in Plasma* (Gordon and Breach)
[40] Landau L D and Lifshitz E M 1991 *Quantum Mechanics: Non-Relativistic Theory* (Butterworth-Heinemann)
[41] Landau L D and Lifshitz E M 1975 *The Classical Theory of Fields: Volume 2* (Butterworth-Heinemann)
[42] Kobzarev I Y and Okun' L B 1968 On the photon mass *Sov. Phys. -Usp.* **11** 338
[43] Esirkepov T Z, Bulanov S V, Yamagiwa M and Tajima T 2006 Electron, positron and photon wakefield acceleration: trapping, wake overtaking and ponderomotive acceleration *Phys. Rev. Lett.* **96** 014803
[44] Kando M *et al* 2007 Demonstration of laser-frequency upshift by electron-density modulations in a plasma wakefield *Phys. Rev. Lett.* **99** 135001
[45] Panchenko A V, Esirkepov T, Pirozhkov A S, Kando M, Kamenets F F and Bulanov S V 2008 Interaction of electromagnetic waves with caustics in plasma flows *Phys. Rev. E* **78** 56402
[46] Bulanov S V *et al* 2012 On the breaking of a plasma wave in a thermal plasma. II. electromagnetic wave interaction with the breaking plasma wave *Phys. Plasmas* **19** 113103
[47] Valenta P *et al* 2020 Recoil effects on reflection from relativistic mirrors in laser plasmas *Phys. Plasmas* **27** 032109
[48] Bulanov S V and Sakharov A S 1991 Induced focusing of electromagnetic wave in a wake plasma wave *JETP Letters* **54** 203–7
[49] Matlis N H *et al* 2006 Snapshots of laser wakefields *Nat. Phys.* **2** 749–53
[50] Valenta P, Grittani G M, Lazzarini C M, Klimo O and Bulanov S V 2021 On the electromagnetic-electron rings originating from the interaction of high-power short-pulse laser and underdense plasma *Phys. Plasmas* **28** 122104
[51] Bulanov S V, Esirkepov T, Kando M, Pirozhkov A S and Rosanov N N 2013 Relativistic mirrors in plasmas. Novel results and perspectives *Phys.-Usp.* **56** 429–64
[52] Vincenti H 2019 Achieving extreme light intensities using optically curved relativistic plasma mirrors *Phys. Rev. Lett.* **123** 105001
[53] Svirplys E *et al* 2026 Plasma lens for focusing attosecond pulses *Nat. Photon.* **20** 151–5
[54] Bulanov S V, Kirsanov V I, Pegoraro F and Sakharov A S 1993 Charged particle and photon acceleration by wake field plasma waves in nonuniform plasmas *Laser Phys.* **3** 1078–1087
[55] Lamač M, Valenta P, Chaulagain U, Nejdl J, Jeong T M and Bulanov S V 2026 Coherent attosecond x-ray pulses from beam-driven relativistic plasma mirrors *Phys. Rev. Res.* **8** L022009
[56] Lamač M, Valenta P, Chaulagain U, Nejdl J, Čáp D, Morvai O and Bulanov S V 2026 Theory of beam-driven nonlinear plasma wake and interior waves *Phys. Rev. E* **113** 045209
[57] Landau L D, Bell J S, Kearsley M J, Pitaevskii L P, Lifshitz E M and Sykes J B 2013 *Electrodynamics of Continuous Media* (Elsevier)
[58] Hadjisolomou P, Shaisultanov R, Jeong T M, Valenta P and Bulanov S V 2023 Effect of ultrastrong magnetic fields on laser-produced gamma-ray flashes *Phys. Rev. Res.* **5** 043153
[59] Beloborodov A M 2022 Scattering of ultrastrong electromagnetic waves by magnetized particles *Phys. Rev. Lett.* **128** 255003
[60] Murakami M, Honrubia J J, Weichman K, Arefiev A V and Bulanov S V 2020 Generation of megatesla magnetic fields by intense-laser-driven microtube implosions *Sci. Rep.* **10** 16653
[61] Najmudin Z *et al* 2001 Measurements of the inverse faraday effect from relativistic laser interactions with an underdense plasma *Phys. Rev. Lett.* **87** 215004
[62] Sheng Z M and Meyer-ter-Vehn J 1996 Inverse faraday effect and propagation of circularly polarized intense laser beams in plasmas *Phys. Rev. E* **54** 1833–42
[63] Liseykina T V, Popruzhenko S V and Macchi A 2016 Inverse Faraday effect driven by radiation friction *New J. Phys.* **18** 072001
[64] Park J *et al* 2019 Ion acceleration in laser generated megatesla magnetic vortex *Phys. Plasmas* **26** 103108
[65] Lamač M, Chaulagain U, Nejdl J and Bulanov S V 2023 Generation of intense magnetic wakes by relativistic laser pulses in plasma *Sci. Rep.* **13** 1701
[66] Russell B K, Vranic M, Campbell P T, Thomas A G R, Schoeffler K M, Uzdensky D A and Willingale L 2025 Magnetic field generation in multipetawatt laser-solid interactions *Phys. Rev. Res.* **7** 013294
[67] Daido H, Miki F, Mima K, Fujita M, Sawai K, Fujita H, Kitagawa Y, Nakai S and Yamanaka C 1986 Generation of a strong magnetic field by an intense CO2 laser pulse *Phys. Rev. Lett.* **56** 846–9
[68] Korneev P, d'Humières E and Tikhonchuk V 2015 Gigagauss-scale quasistatic magnetic field generation in a snail-shaped target *Phys. Rev. E* **91** 043107
[69] Santos J J *et al* 2018 Laser-driven strong magnetostatic fields with applications to charged beam transport and magnetized high energy-density physics *Phys. Plasmas* **25** 056705
[70] Gao L, Zhang Y, Ji H, Russell B K, Pomraning G, Griff-McMahon J, Klein S, Kuranz C and Wei M 2025 Record magnetic field generation by short-pulse laser-driven capacitor-coil targets *Appl. Phys. Lett.* **127** 094101
[71] Wagner U *et al* 2004 Laboratory measurements of 0.7 GG magnetic fields generated during high-intensity laser interactions with dense plasmas *Phys. Rev. E* **70** 026401
[72] Kato Y, Mima K and Bulanov S V 2026 *High Power Laser and Plasma Science* (Springer)
[73] Gurevich A V 2007 Nonlinear effects in the ionosphere *Phys.-Usp.* **50** 1091